



Antarctic krill (*Euphausia superba*) distributions, aggregation structures, and predator interactions in Bransfield Strait

Pavane Annasawmy¹ · John K. Horne¹ · Christian S. Reiss² · George R. Cutter² · Gavin J. Macaulay³

Received: 23 April 2022 / Revised: 16 December 2022 / Accepted: 18 January 2023 / Published online: 1 February 2023
© The Author(s), under exclusive licence to Springer-Verlag GmbH Germany, part of Springer Nature 2023

Abstract

The Antarctic krill, *Euphausia superba*, is a major component of the Southern Ocean's ecosystem. Limited high-resolution data on the relative importance of oceanographic processes on the behavioral responses of krill at traditional predator foraging grounds constitutes a major obstacle in the understanding of krill-environment coupling and ecosystem-based management of this resource. Aggregation structures of krill and predator interactions were investigated using active acoustic data collected by WBAT echosounders deployed on moorings in two hydrographically different sites in Bransfield Strait. Near Nelson Island, water flows from the northwest to southeast while Deception Island is influenced by stronger net current velocities from the southwest to northeast. Krill aggregations were identified and then classified in three clusters using a swarm-identification algorithm and hierarchical clustering using aggregation morphological characteristics: acoustic density, mean depth, center of mass, inertia, equivalent area, aggregation index, and proportion occupied. A total of 693 and 736 aggregations were detected at the mooring sites close to Nelson and Deception Islands. The three aggregation categories ranged from high to low densities, evenness, and dispersion and were distributed throughout the water column. Krill aggregation density distribution and mean thickness are influenced by krill mean depth, current velocities and direction. The majority of observed predator dive profiles occurred over the aggregation type with highest krill densities at both Nelson and Deception Islands, and within the first 25 m of the water column. The heterogeneity of krill aggregations potentially impacts predator foraging strategies and predator–krill interactions in the hydrodynamically active Bransfield Strait.

Keywords Predator–prey interactions · Echometrics · Wavelet analysis · GAM · Hierarchical clustering

Introduction

Antarctic krill (*Euphausia superba*; hereafter “krill”) is a cornerstone species of the Southern Ocean's food web with a recent global biomass estimate of nearly 400 million tons (Atkinson et al. 2009). Krill plays a key role in the recycling of minerals including nitrogen, phosphorus, and iron, thereby contributing to the high productivity of the Southern Ocean (Ikeda and Mitchell 1982; Tovar-Sanchez et al. 2007, 2009). As a trophic conduit, krill is an important grazer of

phytoplankton (Ross et al. 1996; Perissinotto et al. 1997; Bernard et al. 2012), a predator of microzooplankton and copepods (Price et al. 1988; Schmidt et al. 2006), and prey for whales (Santora and Veit 2013; Weinstein et al. 2017), seals (Casaux et al. 2004), penguins (Bernard and Steinberg 2013), and other seabirds (Hunt et al. 1990; Joiris and Dochy 2013). Environmental factors such as frontal zones, tidal regimes (Bernard and Steinberg 2013; Bernard et al. 2017), shelf break and bank bathymetry (Murphy et al. 1997), sea ice cover (Reiss et al. 2017), water circulation (Ichii et al. 1998; Piñones et al. 2013), and oxygen concentrations (Catalán et al. 2008) influence krill densities and aggregation structures. Despite Antarctic krill being distributed over a wide circumpolar belt south of the Polar Front (Ichii et al. 1998; Atkinson et al. 2008), high density aggregations can be regionally distributed (Marr 1962; Laws 1985).

One region with high yet heterogenous krill density, Bransfield Strait (Fig. 1a), is an area of krill recruitment (Siegel and Loeb 1995) and a major krill fishing ground

✉ Pavane Annasawmy
angelee-pavane.annasawmy@ird.fr

¹ School of Aquatic and Fisheries Sciences (SAFS) and Cooperative Institute for Climate, Ocean and Ecosystem Studies (CICOES), University of Washington, Seattle, USA

² Antarctic Ecosystem Research Division, NOAA Southwest Fisheries Science Center, La Jolla, CA, USA

³ Institute of Marine Research, Bergen, Norway

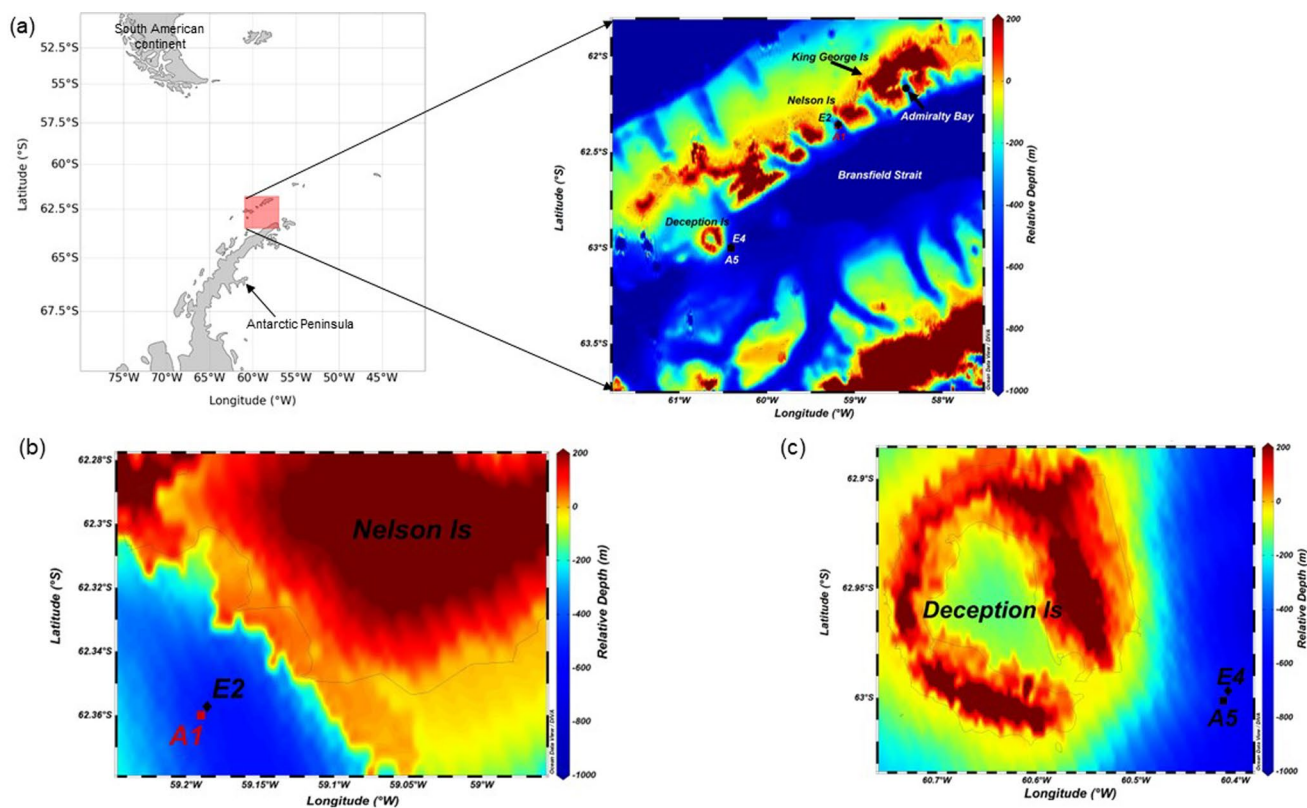


Fig. 1 **a** Regional location of the study sites (red rectangle) with respect to the Antarctic Peninsula and South American continent (in gray). Deployment location of moorings in Bransfield Strait and calibration of echosounders in Admiralty Bay (black dot). **b** Deployment of Mooring 1 ADCP (A1, red square) and Mooring 2 echosounder (E2, black diamond) off Nelson Island and **c** Mooring 5 ADCP (A5,

black square), and Mooring 4 echosounder (E4, black diamond) off Deception Island. The mooring locations are plotted on GEBCO's (General Bathymetric Chart of the Oceans) gridded bathymetric dataset (relative depth below the sea surface in m) (GEBCO Compilation Group 2020) in Ocean Data View software (Schlitzer 2020)

with recent catch allocations of approximately 155 000 t annually (Weinstein et al. 2017; Santa Cruz et al. 2018). The Antarctic krill fishery is managed by the Commission for the Conservation of Antarctic Marine Living Resources (CCAMLR) in a precautionary manner that recognizes the critical role of krill in the Antarctic, the uncertainties associated with krill population dynamics, the potential competition between predators and the fishery, and climate change (CCAMLR 2018). Krill are consumed by a wide predator base (Hunt et al. 1990) and the Antarctic krill fishery overlaps in space and time with areas utilized by these predators (Hinke et al. 2017). As an example, the fishery occurs close to Deception and Nelson Islands (Weinstein et al. 2017) and breeding pairs of Chinstrap (*Pygoscelis antarcticus*) and Gentoo (*Pygoscelis papua*) penguins that forage on krill have been documented on Nelson Island (Trivelpiece et al. 1987; Pfeifer et al. 2019). Humpback whales (*Megaptera novaeangliae*) also prey on krill aggregations in Bransfield Strait, with the whales' distribution linked to bathymetric and hydrographic processes that aggregate krill (Santora et al. 2010).

For ecosystem-based fishery management in the Antarctic, it is important to have current and accurate information on krill aggregation and biomass patterns that support efforts to balance human and animal predator requirements in areas and times that may require conservation (Kock 2000). Surveys of krill distribution and abundance/biomass are traditionally conducted using acoustic systems on research or commercial vessels over temporal scales of weeks to months (Reiss et al. 2021). Scientific and management requirements to extend survey durations and to reduce data collection costs have increased pressures to shift from vessel-based to alternate platforms (e.g., moorings and gliders) (Reiss et al. 2021; Cutter Jr. et al. 2022). Alternate platforms such as moorings collect oceanographic and acoustic data at high resolutions without continuous mobilization of people and vessels over extended periods. Moorings, relative to large research vessels, can be deployed for long periods, and although the spatial coverage of an individual mooring is small, distributed arrays of moorings can provide wide spatial coverage.

The primary objective of this study is to characterize distribution of krill aggregations and associated predator dive profiles using stationary echosounder data from moorings deployed close to Nelson and Deception Islands in Bransfield Strait, Antarctica. Specific objectives include investigating (1) flow patterns at Nelson and Deception Islands, (2) categories of krill aggregation types, (3) biological and environmental influences on krill aggregation attributes, and (4) predator-krill interactions.

Methods

Study sites and mooring deployments

Nine moorings were deployed in Bransfield Strait from January 19 through February 13, 2019 (Krafft et al. 2019). Moorings 2 (Nelson Island) and 4 (southeast of Deception Island) were equipped with Simrad Wide Band Autonomous Transceiver (WBAT) echosounders and ES70 transducers (Kongsberg 2021) (Fig. 1a, Table 1). Mooring 1 was equipped with a Nortek Signature100 (Nortekgroup 2021a) that includes an Acoustic Doppler Current Profiler (ADCP) with an echosounder. Mooring 5 included a Signature250 current profiler (Nortekgroup 2021b). Acoustic data from upward-looking Simrad WBAT echosounders affixed to Moorings 2 and 4 (E2 and E4, hereafter), and water flow data from Nortek Signature100 and Signature250 fixed on Moorings 1 and 5 (A1 and A5, hereafter) were used in this study (Table 1). Moorings 1 and 2 (A1–E2) were deployed at water depths of 324 m and 356 m near Nelson Island (Fig. 1b), while moorings 4 and 5 (E4–A5) were deployed near Deception Island at water depths of 338 m and 150 m (Fig. 1c). All mooring pairs were spaced approximately 1 km apart.

Data acquisition and analyses

Water velocity

The ADCP of the Signature100 on Mooring 1 transmitted and recorded 37 pings at 6 s intervals, every 10 min. Current profiling used 38 depth cells of 10 m each with a blanking distance from the transducer of 2 m to exclude transducer received saturation. Mooring 5 had upward- and downward-looking Signature250 units but only the upward-looking ADCP data stream was used in this study. The upward-looking ADCP was configured to transmit 75 pings at 3 s intervals, repeating the sequence every 10 min. Current profiling was set for 54 depth cells of 4 m each with a blanking distance of 0.5 m.

For data processing and analyses, Signature100 ADCP data were binned in 1-h horizontal and 10-m vertical cells. Signature250 ADCP data were binned in 10-min horizontal by 4-m vertical cells. Both the Signature100 and Signature250 ADCP data were filtered to exclude currents $\geq 1.5 \text{ m s}^{-1}$. Water velocities were temporally matched to the echosounder data to investigate the effect of water flow on krill aggregation characteristics. Although sampling resolutions of the ADCPs and echosounders were not identical, water velocity did not vary within temporal bins, allowing for temporal matching of ADCP and echosounder data.

Echosounder calibration

The WBAT echosounders were calibrated on February 16 while anchored in Admiralty Bay, off King George Island (Fig. 1a) using a standard 38.1 mm tungsten carbide calibration sphere (with 6% cobalt binder) following Demer et al. (2015). During calibration, transducers were deployed at approximately 2-m depth with the sphere suspended approximately 7.5 m below. The Simrad EK80 software was used to obtain echosounder calibration parameters (Table 2) that were used in data processing. The average speed of sound in water between 50, 150, and 300 m depths

Table 1 Overview of the mooring configurations at Nelson and Deception islands

Mooring ID	1	2	4	5
Equipment	Signature100	WBAT	WBAT	Signature250
Deployment area	Nelson Island	Nelson Island	Deception Island	Deception Island
Deployment latitude	S62° 21.634'	S62°21.4379'	S62°59.8140'	S63° 00.0761'
Deployment longitude	W059° 11.4371'	W059°11.1419'	W060°24.4440'	W60° 24.7376'
Echosounder depth (m)	324	356	338	150
Bottom depth (m)	545	588	571	590
Nominal operating frequency (kHz)	70, 120, 70–120 chirp	70	70	250
Nominal transducer beamwidth (°)	10	18	18	NA
Dataset used in this study	ADCP (labeled A1)	Echosounder (labeled E2)	Echosounder (labeled E4)	ADCP (labeled A5)

Table 2 Transducer frequencies and transceiver settings of echosounders E2 and E4

Echosounders	E2	E4
Frequency (kHz)	70	70
Transducer type	Simrad ES70-18CD	Simrad ES70-18CD
Transceiver type	Kongsberg Maritime WBAT	Kongsberg Maritime WBAT
Transmit power (W)	225	225
Pulse duration (ms)	1.024	1.024
Mean Sound speed (m s^{-1})	1452.2	1451.5
Transducer gain (dB)	19.8	19.8
3 dB Beamwidth alongship ($^{\circ}$)	19.6	19.4
3 dB Beamwidth athwartship ($^{\circ}$)	20.3	20.0
Equivalent beam angle (dB)	– 13.0	– 13.0
Sa correction (dB)	0.0	0.0

was calculated using the Chen-Millero equation (Chen and Millero 1977) from salinity and temperature data collected from CTD profiles conducted at the mooring sites. Values were $1452 \pm 2.34 \text{ m s}^{-1}$ (mean \pm standard deviation, hereafter ‘mean \pm SD’) at A1-E2 (Nelson Island) and $1451 \pm 1.21 \text{ m s}^{-1}$ (mean \pm SD) at A5-E4 (Deception Island).

Acoustic data collection and processing

The WBATs were programmed to transmit a 70 kHz continuous wave of 1.024 ms pulse at a pulse repetition rate of 0.9 s for a period of approximately 74 min every 141 min (i.e., “on” for 74 min and then “off” for 67 min). Data were processed using Echoview software (v. 12.0.337) within 16 m of the surface to a depth of 200 m, an arbitrary range designed to exclude surface turbulence and to include krill targets (Siegel 2005). A vertical resolution of 1.9 m and a horizontal resolution of 250 pings (i.e., 5-min bins) were used to estimate krill densities. Ambient noise was removed by applying the background noise removal tool in Echoview (De Robertis and Higginbottom 2007) with the maximum noise set to – 125 dB re $\text{m}^2 \text{m}^{-3}$ (hereafter dB) and the minimum signal-to-noise ratio set at 10 dB.

Krill aggregation characterization

To detect krill aggregations observed in echograms and to develop a classification typology, we used the SHAPES (i.e., shoal analysis and patch estimation system) algorithm (Coetzee 2000) implemented within the Echoview school detection module. Aggregation parameter values (Table 3) were set to detect krill aggregations within the E2 and E4 data. To enable comparison with previous studies (e.g., Tarling et al. 2009; SG-ASAM 2017), the minimum total school height, minimum candidate height, and maximum vertical linking distance were set at 2 m, 1 m, and 5 m, respectively. Aggregations from E2 and E4 were detected at thresholds of – 70 dB (following recommendations from SG-ASAM (2005, 2017) and Amakasu et al. (2011)), and then exported for further analyses.

Hierarchical cluster analyses and ordination were conducted using R packages ade4 (Dray and Dufour 2007), vegan (Oksanen et al. 2019), factextra (Kassambara and Mundt 2020), and dendextend (Galili 2015) to characterize and classify krill aggregations. Using E2 and E4 data, aggregations assumed to be krill, were clustered using numerical and morphological characteristics: areal density

Table 3 Aggregation detection parameters used for E2 and E4 data series

Echoview Attribute	Characteristic	Parameter value
Distance mode	Determine distance for all aggregation detection settings	Ping number
Minimum total school height (m)	After linking is completed, aggregations shorter than the set value will not be included in detections	2
Minimum candidate length (pings)	Minimum length allowed for a single aggregation candidate	50
Minimum candidate height (m)	Minimum height allowed for a single aggregation candidate	1
Maximum vertical linking distance (m)	Maximum vertical distance allowed between two aggregation candidates being linked to form an aggregation	5
Maximum horizontal linking distance (pings)	Maximum horizontal distance allowed between two aggregation candidates being linked to form an aggregation	50
Minimum total school length (pings)	After linking is completed, aggregations shorter than this length will not be included in detections	50

(NASC: Nautical Area Scattering Coefficient; units: dB re $1 \text{ m}^2 \text{ nmi}^{-2}$), mean depth (units: m), center of mass (units: m), inertia (units: m^2), equivalent area (units: m^2), aggregation index (units: m^{-1}), and proportion occupied (cf. Urmy et al. 2012 for metric details). To enable comparison with the results from Tarling et al. (2009), all variables were log transformed ($\log(X + 1)$) and a resemblance matrix of E2 and E4 data were calculated using the Bray–Curtis similarity coefficient. Ward’s clustering method (Ward 1963), which is least susceptible to chaining (Padilla et al. 2007) among aggregations (i.e., clusters growing progressively with the addition of individual aggregations), was used. In contrast to Tarling et al. (2009) who grouped aggregations into classes using the first and second levels of dendrogram division following a hierarchical clustering, the “fviz-nbclust” function (within NbClust package v. 3.0; Charrad et al. 2014) was used to determine the optimum number of clusters. This function determined the best number of clusters to be 3 by comparing the output of several indices (Charrad et al. 2014). Aggregations that belong to the same class type are clustered in a 2-dimensional factorial map. The axes of the factorial map correspond to the eigenvalues. A principal component analysis (PCA) was used to investigate the relative contribution of morphological and Echometric variables to the loadings of the component axes.

Predator dive characterization

Echograms from E2 and E4 were visually inspected to identify and record the number of predator dives throughout the data. Descriptors used to characterize predator dives included: maximum dive depth, presence/absence of krill aggregation(s) directly below the predator dive profile and krill aggregation type. A predator dive was identified by a descent, time at depth, and an ascent forming part or all of a ‘U’, ‘V’, or ‘W’-shaped echo that started and returned to the surface (e.g., Schreer et al. 2001; Viviant et al. 2014). A ‘U’-shaped dive consisted of a descent to depth, a bottom phase spent at maximum depth, and an ascent to the surface. A ‘V’-shaped dive echo consisted of only a descent and an ascent (e.g., Schreer et al. 2001). ‘W’-shaped dives consisted of a descent, a succession of ascending and descending steps at depth (i.e., wiggles), and an ascent (e.g., Viviant et al. 2014). Not all dive profiles were complete in the acoustic record as some predators moved through the acoustic beam. Full and partial dive profiles were counted and investigated relative to the presences of krill aggregation types.

Data visualization and statistical analyses

Prior to running statistical tests, assumptions of normality using the Shapiro Wilk’s test (Shapiro and Wilk 1965) and homogeneity/homoscedasticity of variances using the

Bartlett test (Bartlett 1937) were conducted and verified on the un-transformed mean S_v (i.e., ensemble returned energy), NASC, inertia, equivalent area, mean depth, and center of mass of aggregations. Kruskal Wallis (KW; Hollander and Wolfe 1973) tests were computed (R v. 4.1.2) to investigate differences among aggregation types. The latter test was also used to investigate differences in predator dive frequency among aggregation types. A significance level of 0.05 was chosen to test the null hypotheses that no significant differences exist among aggregation types and that no significant differences exist in the number of predator dives among aggregation types.

Wavelet analysis (Torrence and Compo 1998) was used to identify dominant temporal scales in krill aggregation mean acoustic backscatter (i.e., S_v) data from E2 and E4 datasets. Wavelet power was calculated using the R package WaveletComp (Rösch and Schmidbauer 2018) with a continuous Morlet mother wavelet function (Torrence and Compo 1998). Peaks in the wavelet spectra indicate periods that contribute the most to the variance of the series (Cazelles et al. 2008). Statistical significance in each localized wavelet power was evaluated through comparison to a white noise background spectrum (i.e., a flat Fourier spectrum) defined using 100 simulations to establish a 95% confidence level for the significance of a peak in the wavelet power spectrum (Torrence and Compo 1998).

To investigate the relative importance of candidate covariates influencing krill aggregation mean thickness (i.e., distance of the aggregation in the z dimension) and density distribution ($NASC \times \frac{\text{Inertia}}{\text{Equivalent area}}$), general additive models (GAMs) using restricted maximum likelihood and double penalty approach (Marra and Wood 2011) were constructed using the R package mgcv (v. 1.8.38; Wood 2011). Prior to running the GAMs, a scatterplot matrix using the R package GGally (v. 2.1.2; Schloerke et al. 2021) was plotted to investigate the distribution of each variable and pairwise relationships among them using Pearson’s correlation coefficient. GAMs were used since they do not assume normality and linearity, and are flexible to the statistical distribution of the data (Murase et al. 2009). Similar modeling approaches have been used to investigate relationships between krill acoustic and environmental data (e.g., Trathan et al. 2003; Cox et al. 2009; Murase et al. 2009; Dorman et al. 2015).

A GAM was fitted for each krill aggregation thickness and density distribution at Nelson and Deception Islands using a Gaussian error distribution and an identity-link function. Response variables were log transformed to attain an even spread following inspection of the data distributions (Online Resource 1). Candidate covariates included net current velocities, directions, tides (neap and spring), and mean depth of aggregations. In the GAM,

numerical covariates were modeled as the additive sum of low-rank thin plate regression splines (s) with different basis dimensions (i.e., different k values for each covariate) to achieve the best model fit. The model fit was iteratively checked by varying the k value and calculating the k -index. An index value close to 1 or greater indicates an adequate basis dimension for the smoothing functions. Correlation among variable pairs was investigated using concurvity tests, the nonparametric analog of multicollinearity. Concurvity values range between 0 (no correlation) and 1 (total lack of identifiability) (Wood 2011). None of the covariates and smooth terms showed high degrees of concurvity (≤ 0.3), and they were retained in the final models.

General equations for the GAMs of paired A1-E2 and A5-E4 data are

$$\text{Log}(\text{Mean thickness}) \text{ or } \text{Log} \left(\text{NASC} \times \frac{\text{Inertia}}{\text{Equivalent area}} \right) \\ = s(\text{Net current direction}, \text{Net current velocity}, k = 5) \\ + \text{Tides} + s(\text{Mean depth of aggregations}, k = 3).$$

Assumptions of variance homogeneity and normality were visually assessed using residual plots. Deviance explained (analogous to variance explained in a linear regression) and adjusted r^2 were used as indicators of model performance.

Results

Flow patterns at Nelson and Deception islands

Water flow velocity at A1-E2 near Nelson Island peaked ($0.45 \pm 0.16 \text{ m s}^{-1}$ mean \pm SD, $n = 167$) from January 19 to 25 (mean depths of 147 m) and January 30 to February 9 (mean depths of 127 m) and was low and constant at mean depths of 136 m ($0.12 \pm 0.04 \text{ m s}^{-1}$, $n = 25$) during the rest of the deployment, with water flowing from the northwest to southeast (Fig. 2). The mean \pm SD water flow velocity at E4-A5 near Deception Island was stronger ($0.72 \pm 0.10 \text{ m s}^{-1}$, $n = 23$) from 19 to 23 January and decreased ($0.40 \pm 0.09 \text{ m s}^{-1}$, $n = 132$) through the remainder of the deployment, with water flowing from the southwest to northeast. The net current velocity was more variable with greater amplitudes at Nelson Island compared to Deception Island and was overall stronger at Deception Island.

Aggregation characterization

Mean acoustic backscatter of krill aggregations from Nelson Island has a unimodal distribution ranging from -68 to -50 dB, with a peak at -66 dB and an overall mean of -63 dB ($n = 192$) (Fig. 3). Krill aggregation backscatter data from Deception Island were also unimodal with a main peak at approximately -64 dB (mean $S_v - 62$ dB, $n = 155$).

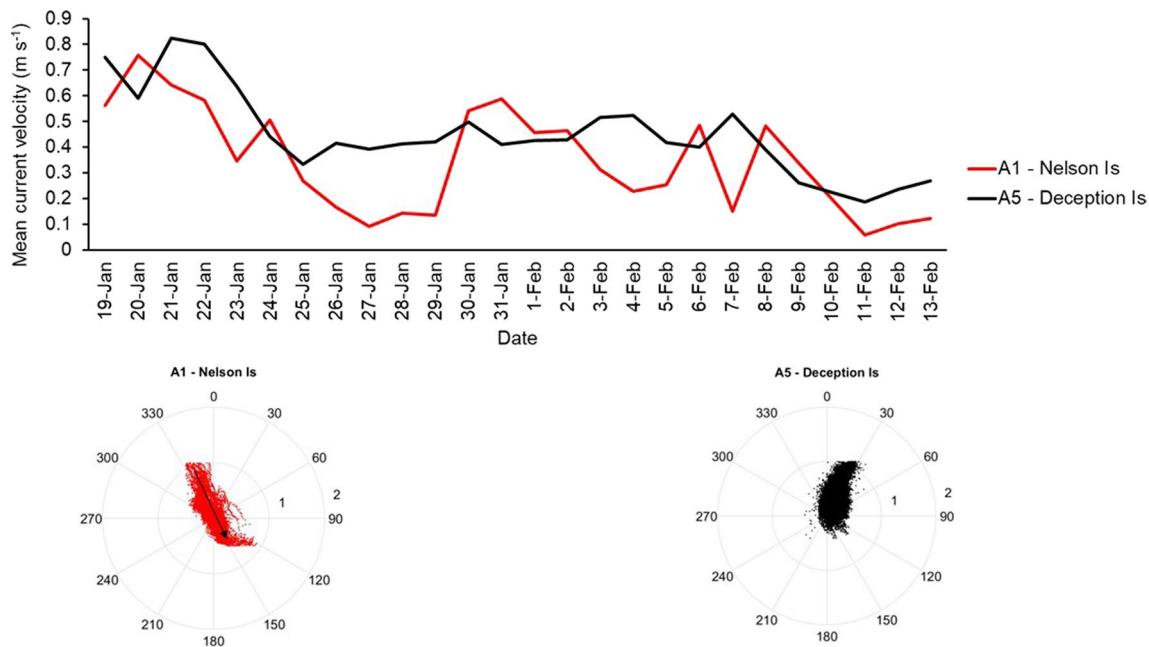


Fig. 2 Top: Net current velocities (m s^{-1}) recorded for the water column above the Nortek Signature100 (A1 at Nelson Island) in red and the Nortek Signature250 (A5 at Deception Island) in black. Bot-

tom: Rose diagrams of the direction (in degrees) of water flow at A1 (shown by the black arrow) and A5, with numbers indicating the magnitude of East and North flows (m s^{-1})

S_v backscatter values were spread over a similar range at Mooring 4 from -67 to -50 dB (Fig. 3).

Krill aggregations from both moorings were grouped in three categories labeled ‘a’ through ‘c’. Ward’s clustering method of the E2 and E4 datasets (Fig. 4a) did not show chaining within or among clusters. Among the 693 aggregations detected for E2, cluster ‘c’ was the least common with 88 aggregations. Clusters ‘a’ and ‘b’ included 281 and 324 aggregations. The three aggregation clusters of E2 differed (Table 4) based on morphological and Echometric aggregation descriptors (KW , $H_{NASC}=492$, $H_{mean\ depth}=22$, $H_{center\ of\ mass}=20$, $H_{inertia}=499$, $H_{proportion\ occupied}=38$, $H_{equivalent\ area}=489$, $H_{aggregation\ index}=489$, $p < 0.05$). Aggregation type ‘a’ was characterized by highest NASC values, the largest mean inertia, and equivalent area values compared to the other types. Type ‘b’ contained the lowest mean NASC, inertia, and equivalent area values (Table 4).

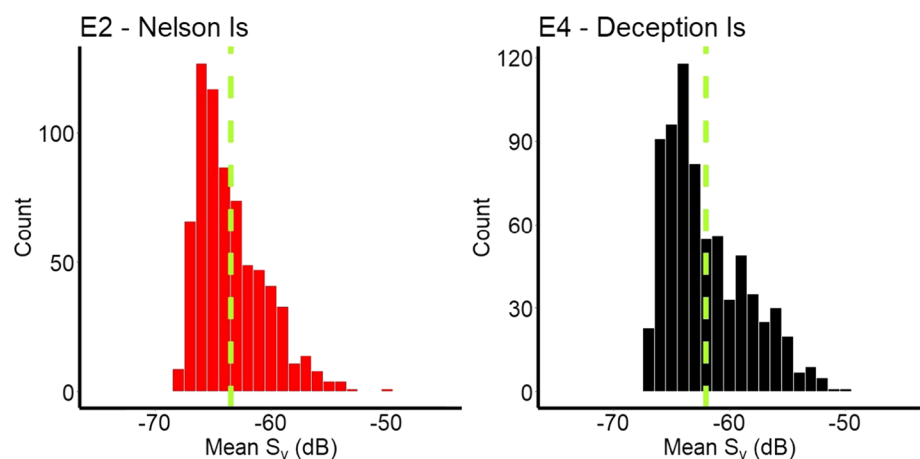
The 736 aggregations detected within the acoustic data from Mooring 4 (i.e., E4) were also assigned to three clusters (‘a’ = 223 aggregations, ‘b’ = 298, and ‘c’ = 215). Aggregation clusters from E4 data were significantly different from each other (Table 4; KW , $H_{NASC}=571$, $H_{mean\ depth}=43$, $H_{center\ of\ mass}=42$, $H_{inertia}=520$, $H_{proportion\ occupied}=82$, $H_{equivalent\ area}=547$, $H_{aggregation\ index}=547$, $p < 0.05$) and grouped similarly to those from E2. Type ‘a’ aggregation contained the highest NASC values and were characterized by the highest inertia and equivalent area values compared to the other aggregation types (Table 4). Type ‘b’ also showed the lowest mean NASC, inertia, and equivalent area values than the other aggregation categories. Type ‘c’ from both E2 and E4 datasets showed intermediate NASC, inertia and equivalent area values. Visual inspection of the echograms showed that all three aggregation types from E2 and E4 were distributed throughout the water column (Fig. 5).

Aggregation type consistency between moorings

PCA analyses identified two principal components (PC) that explained 48% and 29% of the variance in the aggregation properties for E2 and E4 data. The first PC was positively associated with NASC, inertia, and equivalent area (Table 5). The first PC was also negatively associated with proportion occupied and the aggregation index, whereas mean depth and center of mass were dominant variables along the second PC (Fig. 4b). Proportion occupied was the least-dominant variable along both PC axes compared to the other variables (Table 5). The PCA biplots of E2 and E4 krill aggregations illustrate that aggregation type ‘a’ was characterized by high NASC, equivalent area, and inertia, while aggregation type ‘b’ was associated with lower values of these descriptors. The factorial map showed that clusters ‘a’ through ‘c’ clustered mainly along the first PC axis, representing the areal density, inertia (dispersion), and equivalent area (evenness) of the aggregations. Depth was a contributing factor to aggregation variability along the second PC axis. Aggregation types ‘a’ through ‘c’ varied in terms of their absolute values of mean areal density, inertia, and equivalent area (Fig. 4b) but were similar with strong overlap among aggregations on the PCA biplot of Nelson and Deception Islands (Fig. 4c). Overall, the general trends in the aggregation types ‘a’ through ‘c’ were similar across the study sites at Nelson and Deception Islands (Online Resource 2, Fig. 5).

Periodicity of krill acoustic backscatter (i.e., mean S_v) values was variable across temporal scales and among moorings (Fig. 6a, b). In the E2 time series, statistically significant daily periodicity occurs from 13 bins (i.e., 1.1 h), with a peak at 52 bins (i.e., 4.3 h) (Fig. 6a). Significant daily periodicity was also observed within E4 data from 11 bins (i.e., 0.9 h), with a peak at 23 bins

Fig. 3 Frequency distributions of mean S_v (dB) of aggregations detected from E2 (Nelson Island) in red and E4 (Deception Island) in black, with the means of each distribution shown with the green-dashed lines



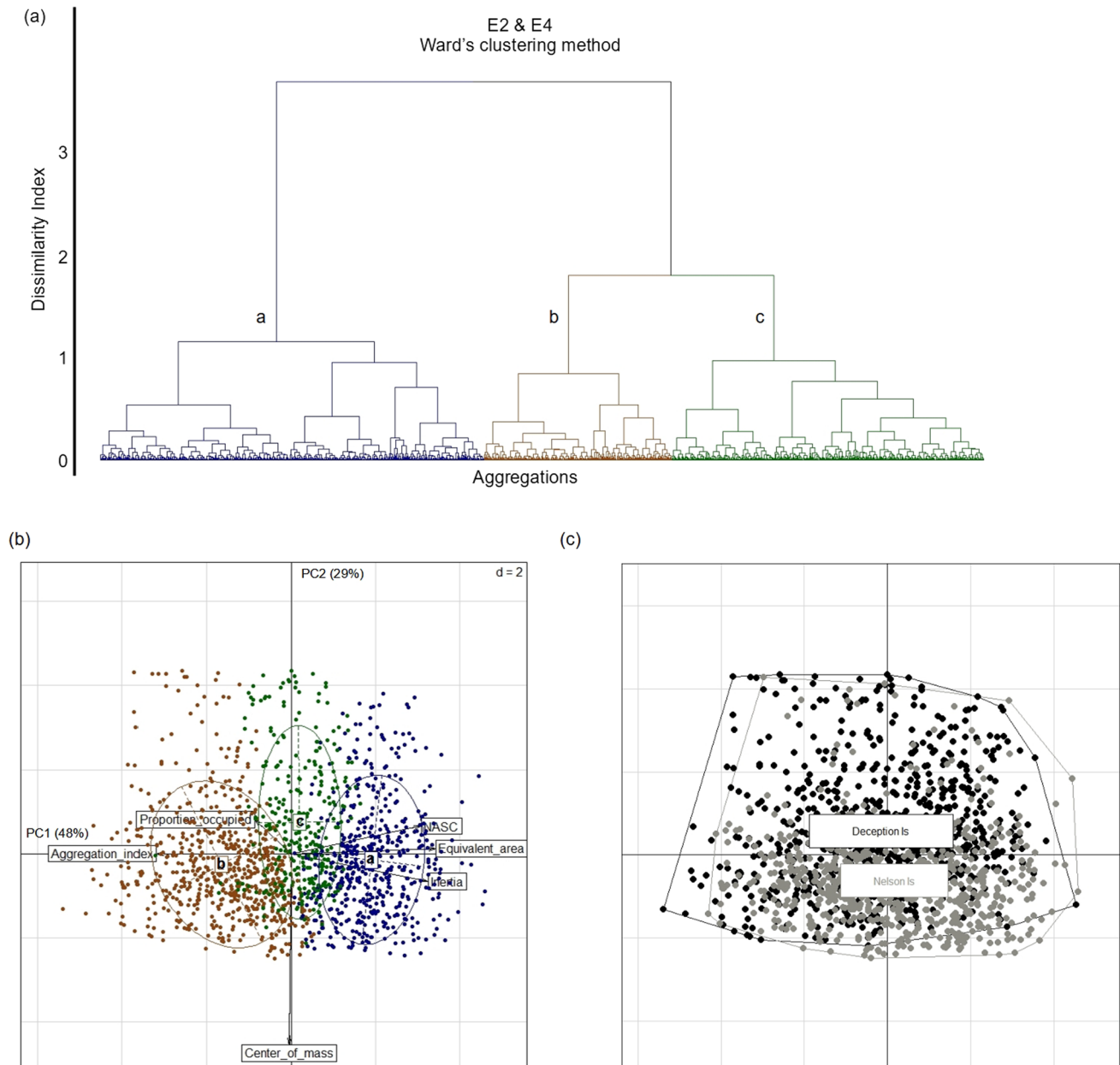


Fig. 4 **a** A dendrogram using Ward's clustering method showing the relative level of dissimilarity between the 693 aggregations detected from E2 (Nelson Island) and 736 aggregations detected from E4 (Deception Island). **b** Principal component (PC) analysis biplots of E2 and E4, with the 2 major axes (PC1 and PC2). Krill aggregations (i.e., 1.9 h) (Fig. 6b). These results emphasize the non-stationary behavior of krill aggregations at Nelson and Deception Islands, and the absence of a single persistent mode of variability throughout the time series.

Predator dives

Predator dives were 'U,' 'V,' or 'W' shaped within the acoustic record (Fig. 7). A total of 1145 'U,' 'V,' or 'W'-shaped

were grouped into three clusters labeled 'a,' 'b,' and 'c'. The direction and length of the arrows mark the direction and rate of steepest increase of the given variable. **c** Krill aggregations were clustered according to the site of the mooring location (Nelson Island and Deception Island)

predator dives were recorded from January 19 through February 13 from E2 near Nelson Island. Approximately 78% of these dives occurred directly above/ through krill aggregations or over diffuse backscatter. The remaining 21% of predator dive profiles occurred over 'empty' water. There was a significant difference in the number of predator dives among aggregation types 'a,' 'b,' and 'c' (KW, $H=62$, $p < 0.05$). A larger proportion of types 'a,' 'b,' and 'c' krill aggregations did not have a predator dive in the vicinity (46%, 73%, and

Table 4 Significant descriptors of the three aggregation clusters (mean \pm standard deviation) identified by multivariate hierarchical classification and PCA analysis

Acoustic dataset	Aggregation types	N	NASC (m ² nmi ⁻²)	Inertia (m ²)	Equivalent area (m ²)	Mean depth (m)	Center of mass (m)
E2	a	281	783 \pm 1016	95 \pm 122	3315 \pm 5070	119 \pm 36	118 \pm 36
	b	324	56 \pm 30	5 \pm 5	204 \pm 161	117 \pm 36	117 \pm 36
	c	88	201 \pm 94	11 \pm 7	628 \pm 391	96 \pm 37	96 \pm 38
E4	a	223	1587 \pm 1555	56 \pm 92	2508 \pm 2995	80 \pm 35	81 \pm 35
	b	298	55 \pm 34	3 \pm 3	156 \pm 107	93 \pm 44	94 \pm 45
	c	215	225 \pm 146	12 \pm 11	510 \pm 288	68 \pm 38	69 \pm 38

Table 5 The relative importance of the two principal components (PC1 and PC2) of the principal component analysis, and the correlations of the seven aggregation descriptors to the different components for E2 and E4 data series

Aggregation descriptors	PC1 (48%)	PC2 (29%)
NASC	0.86	0.14
Mean depth	-0.01	-0.99
Center of mass	-0.01	-0.99
Inertia	0.91	-0.14
Proportion occupied	-0.24	0.18
Equivalent area	0.96	0.03
Aggregation Index	-0.89	0

The percentage variation explained by each PC is given in parentheses

66%) compared to aggregations that recorded single or multiple (between 2 to 10) predator dive profiles (Table 6). Of dives occurring over detected aggregations, approximately 67% occurred over high areal density type ‘a’ aggregations (Table 6). Aggregation types ‘b’ and ‘c’ were intermediate to low areal density aggregations, with low inertia and equivalent area, and occurred in conjunction with 10% to 23% of predator dive profiles.

At E4 near Deception Island, a total of 1650 ‘U,’ ‘V,’ or ‘W’-shaped predator dives were recorded with approximately 30% of these dives occurring directly above or through detected krill aggregations, 4% over diffuse backscatter, and the remaining 66% occurring over “empty water column.” There was a significant difference in the number of predator dives among aggregation types ‘a,’ ‘b,’ and ‘c’ (KW, $H=76$, $p<0.05$). A larger proportion of krill aggregation types ‘a,’ ‘b,’ and ‘c’ did not have a predator dive profile in the vicinity (45%, 77%, and 68%) compared to aggregations recording only 1 or multiple dives (Table 6). Similar to the E2 data series, of those dives occurring over detected aggregations, type ‘a’ was the dominant aggregation type (59%). Aggregation types ‘b’ and ‘c’ recorded approximately equal numbers of dive profiles (20% and 21%). At both Nelson and Deception Islands, greater percentages of predator dive profiles occurred

within the first 25 m of the water column (52% and 46%), with smaller percentages occurring within 25–50 m (29%). Only 15% and 19% predator dive profiles occurred between 50 and 75 m at Nelson and Deception Islands, and 4% to 6% occurred deeper than 75 m.

Factors influencing krill aggregations

Krill aggregation thickness and density distribution showed significant relationships with the mean depth at Deception Island, and net current velocity and direction at Nelson Island (Table 7, Fig. 8). Modeling results showed that tides did not influence krill aggregations at both sites ($p>0.05$; Table 7). Aggregation thickness and density distribution were not influenced by mean aggregation depth at Nelson Island ($p>0.05$) and negatively influenced at Deception Island ($p<0.05$), with decreasing aggregation thickness and density distribution at deeper depths. Increasing current velocities and change in direction (from -100° to 100°) led to increasing aggregation thickness and density distribution at Nelson Island ($p<0.05$). At Deception Island, current velocities had no significant relationships with krill aggregation thickness ($p>0.05$), but led to increasing density distributions ($p<0.05$). Krill aggregation density distribution decreased by a current direction change of 50° to the west–south–west, while it increased by a current direction change of 50° to the south–south–west. Nonlinear and variable relationships between krill and current velocities, directions, and depth at both study sites suggest that complex interactions among physical variables work in concert to influence the thickness and density distributions of krill aggregations.

Discussion

Environmental influences on aggregations at Nelson and Deception islands

Flow patterns likely influenced the size, shape, and density distribution of krill aggregations. Deception and Nelson

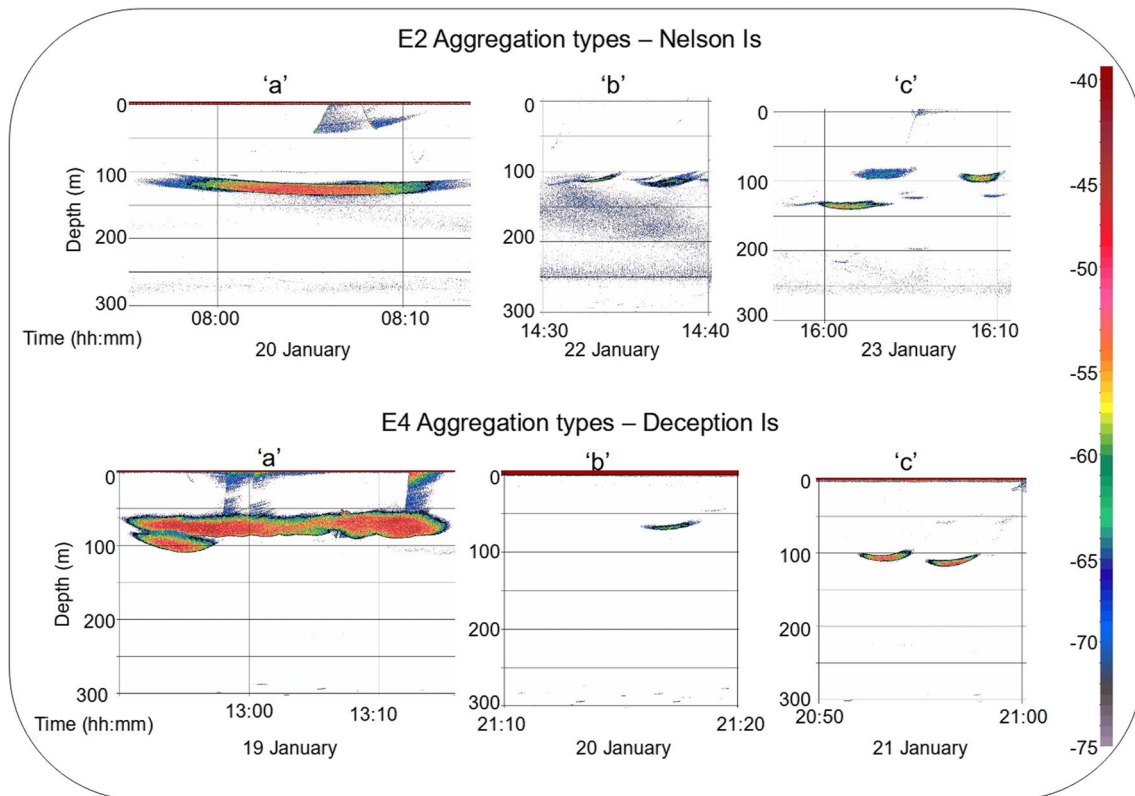


Fig. 5 E2 and E4 example echograms from the surface (0 m) to 300 m showing aggregation types ‘a,’ ‘b,’ and ‘c’ outlined in black using the Echoview school detection module. Color represents S_v (dB)

Islands are within the South Shetlands archipelago and are characterized by complex circulation patterns and steep bathymetric gradients (Niller et al. 1991; Zhou et al. 2002, 2006). Water flow from the southwest to northeast at Deception Island corresponds to Bransfield current (Niller et al. 1991). Nelson Island is located in a more tidal area with water flowing from the northwest to southeast. At mooring pairs A1–E2 (Nelson Island) and E4–A5 (Deception Island), current velocities up to 1 m s^{-1} led to dense and horizontally elongated krill aggregations. Current velocities up to 1.5 m s^{-1} also led to dense krill aggregations at Deception Island. Spring and neap tides had no influence on krill aggregation thickness and density distribution in this study, possibly owing to the coarse resolution of the tidal data used in the GAMS. Biophysical coupling of krill in the Southern Ocean has been previously reported, with currents concentrating krill at Nelson and Deception Islands consistent with those observed at Palmer Station in the Antarctic Peninsula where surface currents interacting with bathymetry can transport and accumulate krill toward nearshore waters or disperse aggregations (Bernard et al. 2017).

In addition to physical factors shaping biological variability, krill mobility will affect the shape and size of aggregations. Krill can maintain their position against current

velocities up to 0.15 m s^{-1} (Macaulay et al. 1984). Various studies report that krill can maintain horizontal sustained swimming speeds of 0.2 m s^{-1} for aggregations with individuals of 45.4 mm in length (Hamner 1984; Brierley and Cox 2010), and they are able to swim into currents for several hours at speeds of 0.17 m s^{-1} (Johnson et al. 1984). Over periods of days to weeks, krill were found to maintain swimming velocities of $0.2\text{--}0.4 \text{ m s}^{-1}$ (Macaulay et al. 1984). An accumulating body of evidence suggests that krill interact strongly and adapt to prevailing shelf-break current regimes and seasonal current patterns (Mackas et al. 1997). Since current speeds at A1–E2 and E4–A5 generally exceeded 0.2 m s^{-1} , krill are expected to only be able to maintain position during slack tide periods. This assumption is consistent with results observed in wavelet plots, as no krill patch was stationary at the mooring sites through the temporal series.

Variability among krill aggregation types

Aggregative behavior is common in krill (Hamner 1984) and has been described using numerous classification schemes including layers, super-patches, and diffuse “clouds” (Kalinowski and Witek 1985); discrete and irregular aggregations (Watkins and Brierley 2002); and small, standard,

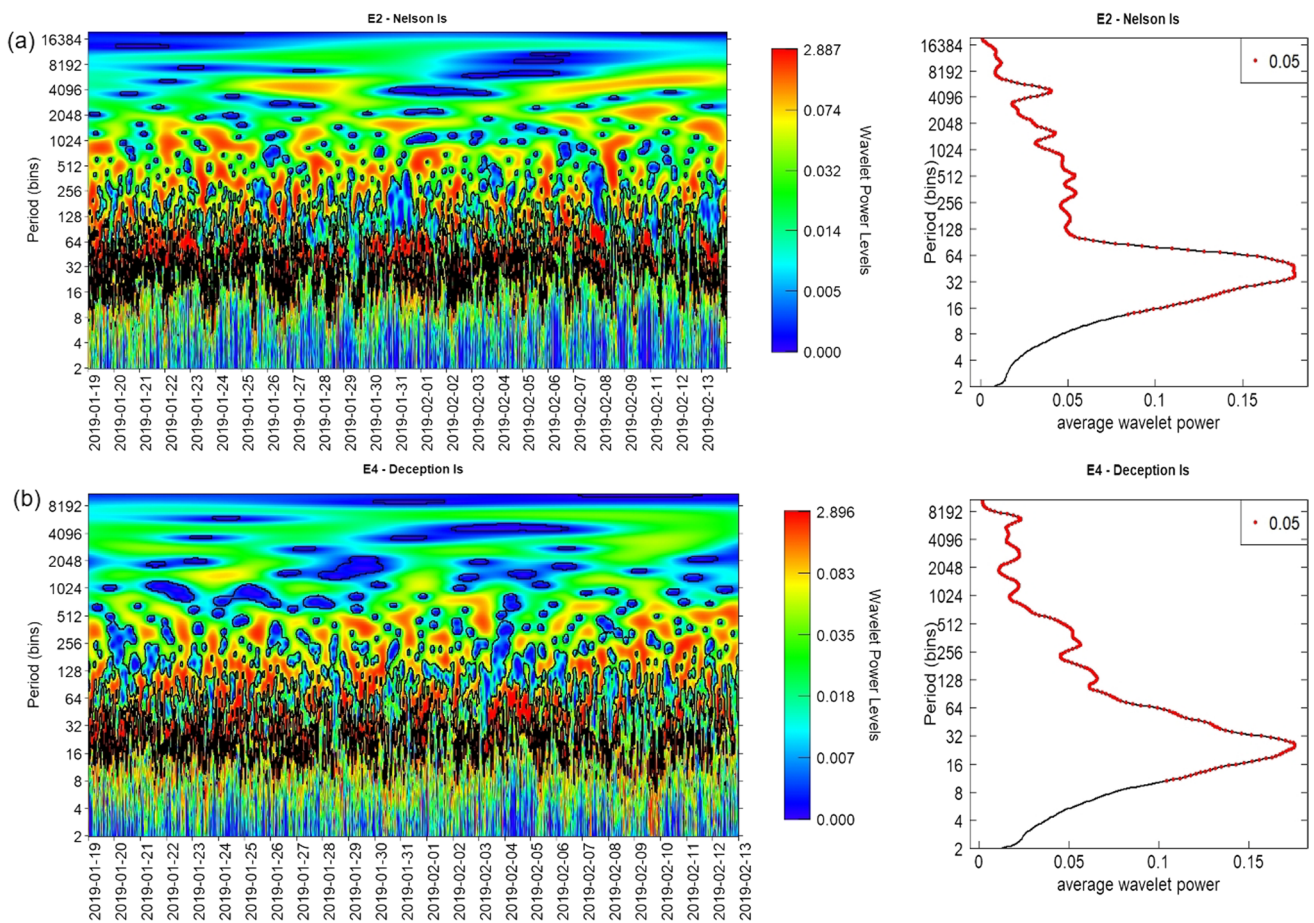


Fig. 6 Left: Wavelet power spectra of mean S_v of krill backscatter from **a** E2 (Nelson Island), and **b** E4 (Deception Island). The color scales represent the quantiles of the distributions of wavelet power levels (σ^2), with low power values represented in blue, and high power values in red; black contour lines indicate areas of significance

(95% confidence against white noise). Right: Average wavelet power spectra (global wavelet spectra) throughout the time series. Significant periods (95% confidence against white noise) are shown in red. The left axes are the Fourier periods (in bins), with 12 bins per hour

and large swarms (Tarling et al. 2009). Similarly, a variety of detection methods have been used to identify and classify krill aggregations including visual classification within echograms (Kalinowski and Witek 1985), or school detection algorithms and hierarchical clustering and ordination (Tarling et al. 2009). Despite differences in data acquisition and aggregation detection methods, the preponderance of krill aggregation classification studies all include large aggregations extending over several kilometers, scattered forms comprised of smaller aggregations, and various other classes of intermediate shapes and patterns (Ricketts et al. 1992).

There is no consensus on a universal approach to characterize krill aggregations. Studies characterizing krill aggregations have used a variety of instruments that evolved over manufacturer product generations, using different descriptive metrics, and a range of spatial and/or temporal lag periods, which may all affect comparisons of aggregation types among results. Moving and stationary platforms may differ in horizontal chord lengths of

aggregations, depending on platform speeds and current velocities. While aggregation types identified from alternate platforms will be consistent internally, caution must be taken when comparing types detected from stationary and moving platforms. The combination of the SHAPES and Echometrics metric suites used to characterize krill aggregations are comprehensive but may be sensitive to variations in their values to provide a universal description of aggregation types in Bransfield Strait. The Echoview school detection module used to identify krill aggregations is designed to isolate discrete aggregations with well-defined boundaries (Burgos and Horne 2008), which is not always the case for krill as they also form diffuse clouds not detected by the algorithm. Potential differences in data acquisition and processing methods used among studies potentially obfuscates if resulting differences are due to krill behavioral differences, location-specific environmental conditions, or to differences in measurement and analytic methodologies.

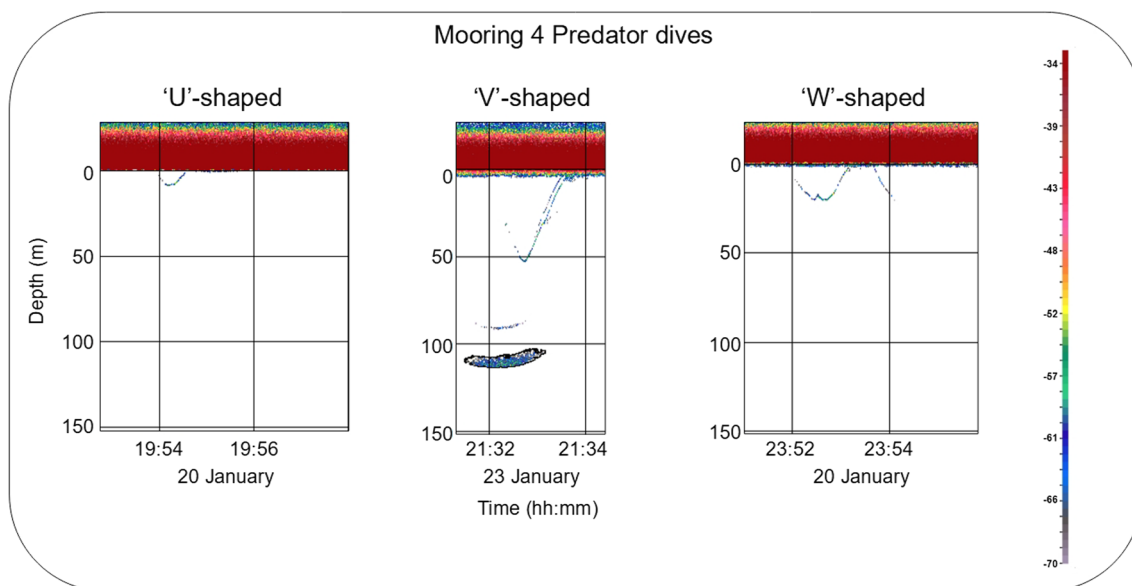


Fig. 7 Mooring 4 example echograms showing ‘U,’ ‘V,’ and ‘W’-shaped predator dives from the surface (0 m). Krill aggregation type ‘b’ is also visible below the ‘V’-shaped dive. Color bar represents S_v (dB)

Table 6 Total number of krill aggregations recording 0, 1 or multiple predator dives at E2 and E4

Echosounder ID	Krill aggregation types	Total number of predator dives	Aggregations with 0 predator dives	Aggregations with 1 predator dive	Aggregations with multiple predator dives
2 (Nelson Is)	a	289	130	80	71 (2–10 dives)
	b	102	237	72	15 (2 dives)
	c	43	58	22	8 (2–4 dives)
	Diffuse backscatter	448			
4 (Deception Is)	a	266	100	57	66 (2–8 dives)
	b	90	229	53	16 (2–5 dives)
	c	95	147	51	17 (2–6 dives)
	Diffuse backscatter	62			

The number of dives for aggregations with multiple predator dives per aggregation type at each site is given in between brackets

As one example, Kalinowski and Witek (1985) recorded four types of krill aggregations in the West Atlantic sector of the Southern Ocean. They described irregular aggregation shapes of several tens of meters high and several hundred thousand meters long. Off the South Shetland Islands, krill were observed to form “super aggregations” of approximately 200 m in at least one dimension and hollow domes, flat sheets, or long-thin ribbons, with the aggregations constantly changing shape and position (Hamner 1984). More recent work identified three aggregation types in the vicinity of the South Shetland Islands (Cox et al. 2010) and in the Western Antarctic Peninsula (Bernard et al. 2017). In the latter, Type I aggregations were larger, shallower, and had higher biomass than Type II aggregations, which were deeper and had the lowest

biomass. Type III aggregations were the smallest type (Bernard et al. 2017). Aggregation types ‘a,’ ‘b,’ and ‘c’ described in this study are similar in densities, but not in their depths, as those identified in Bernard et al. (2017) from an inflatable boat platform. Across studies, general patterns in krill aggregations can be inferred such as long layers and diffuse “clouds,” with a variety of intermediate shapes and forms. Krill are long known to form different types of aggregations depending on their habitat and environmental/biological conditions (Haury et al. 1978). Primary scales of temporal variability in krill distribution also differed between Nelson (significant daily periodicity from 1.1 h and peak at 4.3 h) and Deception Island (significant daily periodicity from 0.9 h and peak at 1.9 h). Since both the environmental and biological conditions differ

Table 7 Results of generalized additive models for comparing aggregation thickness and density distribution to the net current velocity, net current direction, tides, and mean depth of aggregations at Nelson and Deception Islands

Study sites	A1 and E2 (Nelson Island)						E4 and A5 (Deception Island)							
	Response variables	Covariates	edf	Ref.df	F	p	R ²	Deviance explained	edf	Ref.df	F	p	R ²	Deviance explained
Mean thickness	s (current direction, velocity) s (mean depth) Tides		1.71	4	5.21	< 0.05	0.03	3.31%	0.74	4	0.35	> 0.05	0.03	3.66%
			0.01	2	0.005	> 0.05	1.82	2	10.6	< 0.05				
						> 0.05								
Density distribution	s (current direction, velocity) s (mean depth) Tides		1.95	4	30.3	< 0.05	0.16	16.1%	2.59	4	3.69	< 0.05	0.05	5.53%
			0.0007	2	0	> 0.05	1.82	2	8.33	< 0.05				
						> 0.05								

The edf (estimated degrees of freedom), ref.df (estimated residual degrees of freedom), F-statistics, p values, and R² values are given

across the Antarctic Peninsula, it seems plausible that no pair of sites would have identical aggregation patterns.

A variety of factors are known to influence the size and shapes of krill aggregations over space and time. The shape of an aggregation is impacted by organisms balancing access to oxygenated water against predation risk (Hamner 1984; Brierley and Cox 2010). Krill aggregation size may ultimately be constrained by oxygen availability (Johnson et al. 1984), which might explain why very large aggregations (‘super-patches’) were the least common aggregation types identified in this study. The beam diameters of the echosounders and the sampling strategy of switching the WBAT for approximately one hour may also prevent the detection of super-patches of krill. Aggregations are believed to be dynamic features that form and disperse (Hamner 1984; Macaulay et al. 1984; Brierley and Cox 2010). Therefore, any particular aggregation observed is a trade-off among multiple biological and environmental factors such as self-pollution by excretion (Johnson et al. 1984), nearest neighbor distance (Gueron et al. 1996; Tien et al. 2004), tidal regime, surface currents (Bernard and Steinberg 2013; Bernard et al. 2017), and presence of predators (O’Brien 1987). The presence of diving predators would potentially influence krill aggregations due to krill escape reactions. Krill avoid predators by adopting a range of strategies such as “molting” (i.e., shedding their exoskeleton; Hamner 1984) and darting backward (Kils 1979) that result in the contraction or expansion of aggregations (O’Brien 1987).

Predator–prey interactions

Potential predator candidates creating the ‘U,’ ‘V,’ or ‘W’-shaped dives observed on echograms at E2 and E4 may be seals, whales, penguins, and/or other seabirds (Schreer et al. 2001; Burns et al. 2004; Sakamoto et al. 2009; Navarro et al. 2013; Akiyama et al. 2019; Hinke et al. 2021; Annasawmy et al. 2023). These predators were sighted by observers in Bransfield Strait during the survey and penguins were breeding within the vicinity of the study sites (Krafft et al. 2019; Strycker et al. 2020). The ‘V’-shaped dives with no bottom phase over diffuse aggregations or acoustically “empty” water can be further interpreted as search or foraging dives where the predator was unable to locate prey (Chappell et al. 1993). “Wiggles” observed in some of the dive profiles at E2 and E4 may be linked to predators pursuing and capturing prey (e.g., Viviant et al. 2014; Cimino et al. 2016). The greater percentages of predator dive profiles within the first 50 m of the water column are consistent with preferred dive depths of Chinstrap, Adélie, and Gentoo penguins (Chappell et al. 1993; Wilson 2010; Blanchet et al. 2013). Studies have shown that although these penguins can dive down to 100 m, more than 50% of their dives ended at depths less than 40 m (Wilson 2010). Given the characteristics of

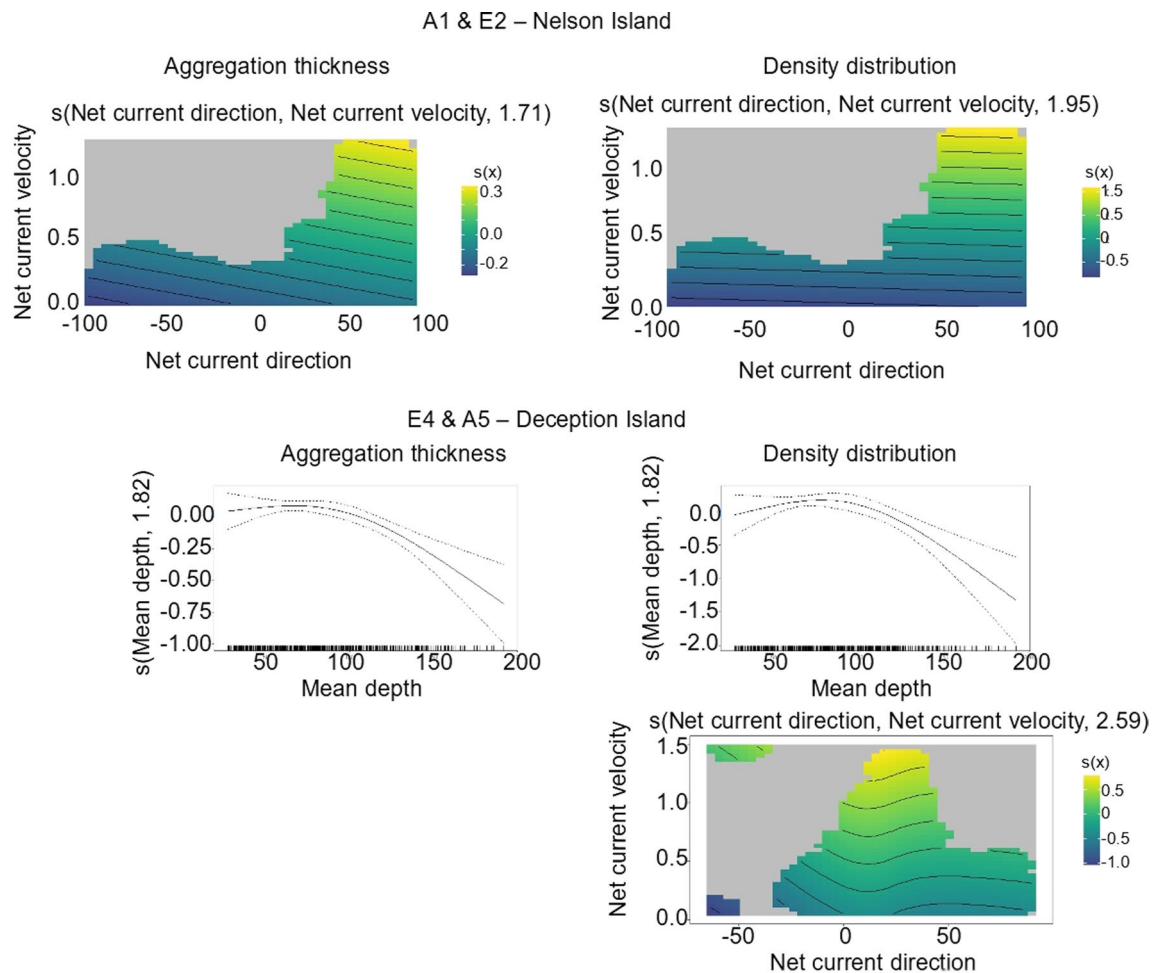


Fig. 8 Smooth functions for the GAMs showing the influence of significant covariates on the aggregation thickness and density of the A1–E2 krill data series at Nelson Island and E4–A5 dataset at Deception Island. The y-axes show the smooth function of each covariate, with the estimated degrees of freedom in brackets. The predicted

models are shown by solid lines and the 95% confidence intervals by dashed lines. Data observations are indicated on the x-axis. Zero on the y-axis corresponds to no effect of the covariate at the corresponding value on the x-axis

whale dive profiles (Croll et al. 2001; Goldbogen et al. 2011; Nowacek et al. 2011; Fais et al. 2016), they would be seen in lower numbers within our upward-looking acoustic beams.

In addition to predator foraging strategies, prey distribution patterns strongly influence predator foraging behavior (Alonzo et al. 2003, Cutter Jr. et al. 2022), with groups of predators feeding more effectively on swarming prey (Hamner 1984). Chinstrap and Adélie penguins were observed to synchronously dive and forage on krill aggregations (Hamner 1984; Hinke et al. 2021). Group foraging behavior (i.e., multiple dive profiles observed over a particular krill aggregation) was observed at Deception and Nelson Islands but is less common than recordings of individual dive profiles. Among detected krill aggregations, type ‘a’ (which had high densities and were evenly spread) had the highest percentage and occurrences of multiple dive profiles compared to the other aggregation types. Type ‘b’ aggregations, which were

low areal density, recorded greater percentages of zero dive profiles than types ‘a’ and ‘c.’ Groups of predators appear to preferentially dive over dense krill aggregations at Nelson and Deception Islands.

While shallow krill aggregations are predicted to attract diving penguins (Chappell et al. 1993; Bernard et al. 2017), we observed that aggregation types with the highest densities, even if not found at the surface, attracted diving predators. Once a dense aggregation type is detected, predators may forage individually and in groups on those aggregations and return to areas where encounter rates with that particular aggregation type was highest (e.g., Santora et al. 2009). The large number of predator dives recorded over diffuse rather than discrete aggregations at Nelson Island is consistent with the observation that most krill predators are believed to target individuals (Brierley and Cox 2010) rather than aggregations, or that these dives are search rather than

foraging dives. At Deception Island, a greater percentage of predator dive profiles occurred over empty water compared to detected krill aggregations. The inferred low successful foraging rates can be attributed to spatial segregation among predators within their foraging ranges (Trivelpiece et al. 1987) that result in longer travel distances within Bransfield Strait to reduce intra- and inter-specific predator competition. If true, then predators would only pass through the E4 acoustic beam close Deception Island during their transit to other prey locations (Hunt et al. 1992).

Biological responses to climate-induced changes in the Southern Ocean may impact both krill dynamics and their predators' foraging success. Future ocean warming is predicted to decrease oxygen levels by 3% for every 1 °C of warming, resulting in krill aggregations becoming smaller or less densely packed (Brierley and Cox 2010), which may further impact predator foraging. Future work will associate predator dive profiles with known predator foraging dive patterns (e.g., Chappell et al. 1993; Schreer et al. 2001; Annasawmy et al. 2023). Rapid and consistent krill aggregation and predator classifications from acoustic data can then be used in simulation models such as the Krill-Predator-Fishery Model (Watters et al. 2013) or the Spatial Multi-Species Operating Model (Plagányi and Butterworth 2006) to predict the krill–predator–fishery interactions in krill management units defined by CCAMLR. When combined with knowledge of regional ocean dynamics, predator-krill surveys would allow critical predator foraging grounds to be identified, and the distribution of catch and fishing effort to be adapted to changes in krill distributions and predator foraging patterns.

Summary

Aggregation patterns of Antarctic krill, *E. superba*, were characterized in two environmentally contrasting sites in Bransfield Strait using 70 kHz data from moored echosounders. Echometrics (Urmy et al. 2012) and hierarchical clustering were used to characterize and classify recorded aggregations. This study showed that krill aggregations respond to environmental and biological factors such as current velocities, directions, and presence of predators, with aggregations that are temporally heterogeneous in density distribution and mean thickness. Detection of predator dive profiles within stationary echogram records illustrated diverse dive shapes and potential foraging strategies. Predator dive profiles and krill aggregations are closely linked, with the predator dives influencing the size and shape of aggregations and the krill densities influencing the predator dive patterns.

Supplementary Information The online version contains supplementary material available at <https://doi.org/10.1007/s00300-023-03113-z>.

Acknowledgements The authors acknowledge the captain, crew, and scientific staff of the RV *Kronprins Haakon* for deployment and recovery of the moorings. The first author is the beneficiary of a post-doctoral research fellowship granted by the Cooperative Institute for Climate, Ocean, and Ecosystem Studies (CICOES, University of Washington, Seattle, USA). This publication is funded by CICOES under NOAA Cooperative Agreement NA200AR4320271, Contribution No. 2023-1251.

Author contributions CSR and GJM conceived and designed this study, and provided data with input from GRC. PA processed and analyzed the data and prepared the figures, advised by JKH. PA wrote the manuscript, JKH, CSR, GRC, and GJM revised the manuscript.

Declarations

Conflict of interest The authors declare that they have no conflict of interest.

Informed consent All authors consent to the publication of this manuscript.

References

- Akiyama Y, Akamatsu T, Rasmussen MH, Iversen MR, Iwata T, Goto Y, Aoki K, Sato K (2019) Leave or stay? Video-logger revealed foraging efficiency of humpback whales under temporal change in prey density. *PLoS ONE* 14:e0211138. <https://doi.org/10.1371/journal.pone.0211138>
- Alonzo SH, Switzer PV, Mangel M (2003) Ecological games in space and time: the distribution and abundance of Antarctic krill and penguins. *Ecology* 84:1598–1607
- Amakasu K, Ono A, Moteki M, Ishimaru T (2011) Sexual dimorphism in body shape of Antarctic krill (*Euphausia superba*) and its influence on target strength. *Polar Sci* 5:179–186. <https://doi.org/10.1016/j.polar.2011.04.005>
- Annasawmy P, Horne JK, Reiss CS, Macaulay GJ (2023) Characterizing Antarctic air-breathing predator dive patterns on a common prey base from stationary echosounders. Submitted to *Polar Science* <https://doi.org/10.21203/rs.3.rs-1586876/v1>
- Atkinson A, Siegel V, Pakhomov E, Rothery P, Loeb V, Ross R, Quentin L, Schmidt K, Fretwell P, Murphy E, Tarling G, Fleming A (2008) Oceanic circumpolar habitats of Antarctic krill. *Mar Ecol Prog Ser* 362:1–23. <https://doi.org/10.3354/meps07498>
- Atkinson A, Siegel V, Pakhomov EA, Jessopp MJ, Loeb V (2009) A reappraisal of the total biomass and annual production of Antarctic krill. *Deep Sea Res Part Oceanogr Res Pap* 56:727–740. <https://doi.org/10.1016/j.dsr.2008.12.007>
- Bartlett MS (1937) Properties of sufficiency and statistical tests. *Proc R Soc Lond A* 160:268–282. <https://doi.org/10.1098/rspa.1937.0109>
- Bernard KS, Steinberg DK (2013) Krill biomass and aggregation structure in relation to tidal cycle in a penguin foraging region off the Western Antarctic Peninsula. *ICES J Mar Sci* 70:834–849. <https://doi.org/10.1093/icesjms/fst088>
- Bernard KS, Steinberg DK, Schofield OME (2012) Summertime grazing impact of the dominant macrozooplankton off the Western Antarctic Peninsula. *Deep Sea Res Part Oceanogr Res Pap* 62:111–122. <https://doi.org/10.1016/j.dsr.2011.12.015>
- Bernard KS, Cimino M, Fraser W, Kohut J, Oliver MJ, Patterson-Fraser D, Schofield OME, Statscewich H, Steinberg DK, Winsor P (2017) Factors that affect the nearshore aggregations of Antarctic

- krill in a biological hotspot. *Deep Sea Res Part Oceanogr Res Pap* 126:139–147. <https://doi.org/10.1016/j.dsr.2017.05.008>
- Blanchet M-A, Biuw M, Hofmeyr GJG, de Bruyn PJN, Lydersen C, Kovacs KM (2013) At-sea behaviour of three krill predators breeding at Bouvetøya: Antarctic fur seals, macaroni penguins and chinstrap penguins. *Mar Ecol Prog Ser* 477:285–302. <https://doi.org/10.3354/meps10110>
- Brierley AS, Cox MJ (2010) Shapes of krill swarms and fish schools emerge as aggregation members avoid predators and access oxygen. *Curr Biol* 20:1758–1762. <https://doi.org/10.1016/j.cub.2010.08.041>
- Burgos JM, Horne JK (2008) Characterization and classification of acoustically detected fish spatial distributions. *ICES J Mar Sci* 65:1235–1247. <https://doi.org/10.1093/icesjms/fsn087>
- Burns JM, Costa DP, Fedak MA, Hindell MA, Bradshaw CJA, Gales NJ, McDonald B, Trumble SJ, Crocker DE (2004) Winter habitat use and foraging behavior of crabeater seals along the Western Antarctic Peninsula. *Deep Sea Res II Top Stud Oceanogr* 51:2279–2303. <https://doi.org/10.1016/j.dsr2.2004.07.021>
- Casaux R, Bellizia L, Baron A (2004) The diet of the Antarctic fur seal *Arctocephalus gazella* at Harmony Point, South Shetland Islands: evidence of opportunistic foraging on penguins? *Polar Biol* 27:59–65. <https://doi.org/10.1007/s00300-003-0559-z>
- Catalán IA, Morales-Nin B, Company JB, Rotllant G, Palomera I, Emelianov M (2008) Environmental influences on zooplankton and micronekton distribution in the Bransfield Strait and adjacent waters. *Polar Biol* 31:691–707. <https://doi.org/10.1007/s00300-008-0408-1>
- Cazelles B, Chavez M, Berteaux D, Ménard F, Vik JO, Jenouvrier S, Stenseth NC (2008) Wavelet analysis of ecological time series. *Oecologia* 156:287–304
- CCAMLR (Commission for the Conservation of Antarctic Marine Living Resources) (2018) Krill fisheries and sustainability. <https://www.ccamlr.org/en/fisheries/krill-fisheries-and-sustainability/>. Accessed 13 Sept 2021
- Chappell MA, Shoemaker VH, Janes DN, Bucher TL, Maloney SK (1993) Diving behavior during foraging in breeding adelic penguins. *Ecology* 74:1204–1215
- Charrad M, Ghazzali N, Boiteau V, Niknafs A (2014) NbClust: An R package for determining the relevant number of clusters in a data set. *J Stat Softw* 61:1–36
- Chen CT, Millero FJ (1977) Speed of sound in seawater at high pressures. *J Acoust Soc Am* 62:1129–1135
- Cimino MA, Moline MA, Fraser WR, Patterson-Fraser DL, Oliver MJ (2016) Climate-driven sympatry may not lead to foraging competition between congeneric top-predators. *Sci Rep* 6:18820. <https://doi.org/10.1038/srep18820>
- Coetzee J (2000) Use of a shoal analysis and patch estimation system (SHAPES) to characterise sardine schools. *Aquat Living Resour* 13:1–10. [https://doi.org/10.1016/S0990-7440\(00\)00139-X](https://doi.org/10.1016/S0990-7440(00)00139-X)
- Cox MJ, Demer DA, Warren JD, Cutter GR, Brierley AS (2009) Multi-beam echosounder observations reveal interactions between Antarctic krill and air-breathing predators. *Mar Ecol Prog Ser* 378:199–209. <https://doi.org/10.3354/meps07795>
- Cox MJ, Warren JD, Demer DA, Cutter GR, Brierley AS (2010) Three-dimensional observations of swarms of Antarctic krill (*Euphausia superba*) made using a multi-beam echosounder. *Deep Sea Res II* 57:508–518. <https://doi.org/10.1016/j.dsr2.2009.10.003>
- Croll DA, Clark CW, Calambokidis J, Ellison WT, Tershy BR (2001) Effect of anthropogenic low-frequency noise on the foraging ecology of *Balaenoptera* whales. *Anim Conserv* 4:13–27
- Cutter GR Jr, Reiss CS, Nylund S, Watters GM (2022) Antarctic krill biomass and flux measured using Wideband echosounders and acoustic doppler current profilers on submerged moorings. *Front Mar Sci* 9:784469. <https://doi.org/10.3389/fmars.2022.784469>
- Demer DA, Berger L, Bernasconi M, Bethke E, Boswell K, Chu D, Domokos R, Dunford A, Fässler S, Gauthier S, Hufnagle LT, Jech JM, Bouffant N, Lebourges-Dhaussy A, Lurton X, Macaulay GJ, Perrot Y, Ryan T, Parker-Stetter S, Stienessen S, Weber T, Williamson N (2015) Calibration of acoustic instruments. *ICES Cooper Res Rep* 326:133
- De Robertis A, Higginbottom I (2007) A post-processing technique for estimation of signal-to-noise ratio and removal of echosounder background noise. *ICES J Mar Sci* 64:1282–1291
- Dorman JG, Sydeman WJ, Garcia-Reyes M, Zeno RA, Santora JA (2015) Modeling krill aggregations in the central-northern California Current. *Mar Ecol Prog Ser* 528:87–99. <https://doi.org/10.3354/meps11253>
- Dray S, Dufour A (2007) The ade4 package: implementing the duality diagram for ecologists. *J Stat Softw* 22:1–20. <https://doi.org/10.18637/jss.v022.i04>
- Fais A, Johnson M, Wilson M, Aguilar Soto N, Madsen PT (2016) Sperm whale predator-prey interactions involve chasing and buzzing, but no acoustic stunning. *Sci Rep* 6:28562. <https://doi.org/10.1038/srep28562>
- Galili T (2015) dendextend: an R package for visualizing, adjusting, and comparing trees of hierarchical clustering. *Bioinformatics*. <https://doi.org/10.1093/bioinformatics/btv428>
- GEBCO Compilation Group (2020) GEBCO 2020 grid. <https://doi.org/10.5285/a29c5465-b138-234d-e053-6c86abc040b9>
- Goldbogen JA, Calambokidis J, Oleson E, Potvin J, Pyenson ND, Schorr G, Shadwick RE (2011) Mechanics, hydrodynamics and energetics of blue whale lunge feeding: efficiency dependence on krill density. *J Exp Biol* 214:698–699. <https://doi.org/10.1242/jeb.054726>
- Guéron S, Levin SA, Rubenstein DI (1996) The dynamics of herds: from individuals to aggregations. *J Theor Biol* 182:85–98. <https://doi.org/10.1006/jtbi.1996.0144>
- Hamner WM (1984) Aspects of schooling in *Euphausia Superba*. *J Crustac Biol* 4:67–74. <https://doi.org/10.1163/1937240X84X00507>
- Haury LR, McGowan JA, Wiebe PH (1978) Patterns and processes in the time-space scales of plankton distributions. In: Steele JH (ed) *Spatial pattern in plankton communities*. Springer, Boston, pp 277–327
- Hinke JT, Cossio AM, Goebel ME, Reiss CS, Trivelpiece WZ, Watters GM (2017) Identifying risk: concurrent overlap of the antarctic krill fishery with krill-dependent predators in the Scotia Sea. *PLoS ONE* 12:e0170132. <https://doi.org/10.1371/journal.pone.0170132>
- Hinke JT, Russell TM, Hermanson VR, Brazier L, Walden SL (2021) Serendipitous observations from animal-borne video loggers reveal synchronous diving and equivalent simultaneous prey capture rates in chinstrap penguins. *Mar Biol* 168:135. <https://doi.org/10.1007/s00227-021-03937-5>
- Hollander M, Wolfe DA (1973) *Nonparametric statistical methods*. Wiley, New York, pp 115–120
- Hunt GL, Heinemann D, Veit RR, Heywood RB, Everson I (1990) The distribution, abundance and community structure of marine birds in southern Drake Passage and Bransfield Strait, Antarctica. *Cont Shelf Res* 10:243–257. [https://doi.org/10.1016/0278-4343\(90\)90021-D](https://doi.org/10.1016/0278-4343(90)90021-D)
- Hunt G, Heinemann D, Everson I (1992) Distributions and predator-prey interactions of macaroni penguins, Antarctic fur seals, and Antarctic krill near Bird Island, South Georgia. *Mar Ecol Prog Ser* 86:15–30. <https://doi.org/10.3354/meps086015>
- Ichii T, Katayama K, Obitsu N, Ishii H, Naganobu M (1998) Occurrence of Antarctic krill (*Euphausia superba*) concentrations in the vicinity of the South Shetland Islands: relationship to environmental parameters. *Deep Sea Res Part Oceanogr Res Pap* 45:123–1262. [https://doi.org/10.1016/S0967-0637\(98\)00011-9](https://doi.org/10.1016/S0967-0637(98)00011-9)

- Ikeda T, Mitchell AW (1982) Oxygen uptake, ammonia excretion and phosphate excretion by krill and other Antarctic zooplankton in relation to their body size and chemical composition. *Mar Biol* 71:283–298
- Johnson MA, Macaulay MC, Biggs DC (1984) Respiration and excretion within a mass aggregation of *Euphausia Superba*: implications for krill distribution. *J Crustac Biol* 4:174–184. <https://doi.org/10.1163/1937240X84X00570>
- Joiris CR, Dochy O (2013) A major autumn feeding ground for fin whales, southern fulmars and grey-headed albatrosses around the South Shetland Islands, Antarctica. *Polar Biol* 36:1649–1658
- Kalinowski J, Witek Z (1985) Scheme for classifying aggregations of Antarctic krill. BIOMASS handbook no 27. SCAR/SCOR/IABO/ACMRR, Group of Specialist on Living Resources of the Southern Oceans
- Kassambara A, Mundt F (2020) factoextra: extract and visualize the results of multivariate data analyses (version 1.0.7). <https://CRAN.R-project.org/package=factoextra>
- Kils U (1979) Swimming speed and escape capacity of Antarctic krill, *Euphausia superba*. *Univ Kiel Inst* 27:264–266
- Kock K-H (2000) Understanding CCAMLR's approach to management. https://www.ccamlr.org/es/system/files/science_journal_papers/03constable.pdf. Accessed 21 Feb 2022
- Kongsberg (2021) Simrad WBAT. https://www.kongsberg.com/maritime/products/ocean-science/fishery-research/es_scientific/wbat/. Accessed 30 Aug 2022
- Krafft B, Bakkeplass K, Berge T, Biuw M, Erices J, Jones E, Knutsen T, Kubilius R, Kvalsund M, Lindstrøm U, Macaulay GJ, Renner A, Rey A, Skern R, Sjøiland H, Wienerroither R, Ahonen H, Goto J, Hoem N, Huerta M, Höfer J, Iden O, Jouanneau W, Kruger L, Liholt H, Lowther A, Makhado A, Mestre M, Narvestad A, Oosthuisen C, Rodrigues J, Øyerhamn R (2019) Report from a krill focused survey with RV Kronprins Haakon and land-based predator work in Antarctica during 2018/2019. The Norwegian Ministry of Trade Industry and Fisheries, Oslo, p 107
- Laws RM (1985) The ecology of the Southern Ocean. *Am Sci* 73:26–40
- Macaulay MC, Saunders English T, Mathisen OA (1984) Acoustic characterization of swarms of antarctic krill (*Euphausia Superba*) From Elephant Island and Bransfield Strait. *J Crustac Biol* 4:16–44. <https://doi.org/10.1163/1937240X84X00480>
- Mackas DL, Kieser R, Saunders M, Yelland DR, Brown RM, Moore DF (1997) Aggregation of euphausiids and Pacific hake (*Merluccius productus*) along the outer continental shelf off Vancouver Island. *Can J Fish Aquat Sci* 54:2080–2096. <https://doi.org/10.1139/f97-113>
- Marr JWS (1962) The natural history and geography of the Antarctic krill (*Euphausia superba* Dana). *Discov Rep* 32:33–464
- Marra G, Wood SN (2011) Practical variable selection for generalized additive models. *Comput Stat Data Anal* 55:2372–2387. <https://doi.org/10.1016/j.csda.2011.02.004>
- Murase H, Nagashima H, Yonezaki S, Matsukura R, Kitakado T (2009) Application of a generalized additive model (GAM) to reveal relationships between environmental factors and distributions of pelagic fish and krill: a case study in Sendai Bay, Japan. *ICES J Mar Sci* 66:1417–1424. <https://doi.org/10.1093/icesjms/fsp105>
- Murphy EJ, Trathan PN, Everson I, Parkes G, Daunt F (1997) Krill fishing in the scotia sea in relation to bathymetry, including the detailed distribution around South Georgia. *CCAMLR Sci* 4:1–17
- Navarro J, Votier SC, Aguzzi J, Chiesa JJ, Forero MG, Phillips RA (2013) Ecological segregation in space, time and trophic niche of sympatric planktivorous petrels. *PLoS ONE* 8:e62897. <https://doi.org/10.1371/journal.pone.0062897>
- Niller PP, Amos A, Hu JH (1991) Water masses and 200 m relative geostrophic circulation in the western Bransfield Strait region. *Deep Sea Res A Oceanogr Res Pap* 38:943–959
- Nortekgroup (2021a) Signature100. <https://www.nortekgroup.com/products/signature100>. Accessed 30 Aug 2021a
- Nortekgroup (2021b) Signature250. <https://www.nortekgroup.com/products/Signature250>. Accessed 30 Aug 2021b
- Nowacek DP, Friedlaender AS, Halpin PN, Hazen EL, Johnston DW, Read AJ, Espinasse B, Zhou M, Zhu Y (2011) Super-aggregations of krill and humpback whales in Wilhelmina Bay, Antarctic Peninsula. *PLoS ONE* 6:e19173. <https://doi.org/10.1371/journal.pone.0019173>
- O'Brien DP (1987) Description of escape responses of krill (Crustacea: Euphausiacea), with particular reference to swarming behavior and the size and proximity of the predator. *J Crustac Biol* 7:449–457. <https://doi.org/10.2307/1548294>
- Oksanen J, Blanchet FG, Friendly M, Kindt R, Legendre P, McGinn D, Minchin PR, O'Hara RB, Simpson GL, Solymos P, Stevens MHH, Szoecs E, Wagner H (2019) vegan: community ecology package (version 2.5.6). <https://CRAN.R-project.org/package=vegan>
- Padilla G, Cartea ME, Ordás A (2007) Comparison of several clustering methods in grouping kale landraces. *J Am Soc Hort Sci* 132:387–395
- Perissinotto R, Pakhomov E, McQuaid C, Froneman P (1997) In situ grazing rates and daily ration of Antarctic krill *Euphausia superba* feeding on phytoplankton at the Antarctic Polar Front and the Marginal Ice Zone. *Mar Ecol Prog Ser* 160:77–91. <https://doi.org/10.3354/meps160077>
- Pfeifer C, Barbosa A, Mustafa O, Peter HU, Rümmler MC, Brenning A (2019) Using fixed-wing UAV for detecting and mapping the distribution and abundance of penguins on the South Shetlands Islands. *Antarct Drones* 3:39. <https://doi.org/10.3390/drones302039>
- Piñones A, Hofmann E, Daly K, Dinniman M, Klinck J (2013) Modeling the remote and local connectivity of Antarctic krill populations along the western Antarctic Peninsula. *Mar Ecol Prog Ser* 481:69–92. <https://doi.org/10.3354/meps10256>
- Plagányi E, Butterworth D (2006) A spatial multi-species operating model (SMOM) of krill-predator interactions in small-scale management units in the Scotia Sea. University of Cape Town, Cape Town
- Price HJ, Boyd KR, Boyd CM (1988) Omnivorous feeding behavior of the Antarctic krill *Euphausia superba*. *Mar Biol* 97:67–77. <https://doi.org/10.1007/BF00391246>
- Reiss C, Cossio A, Santora J, Dietrich K, Murray A, Mitchell B, Walsh J, Weiss E, Gimpel C, Jones C, Watters G (2017) Overwinter habitat selection by Antarctic krill under varying sea-ice conditions: implications for top predators and fishery management. *Mar Ecol Prog Ser* 568:1–16. <https://doi.org/10.3354/meps12099>
- Reiss CS, Cossio AM, Walsh J, Cutter GR, Watters GM (2021) Glider-based estimates of meso-zooplankton biomass density: a fisheries case study on antarctic krill (*Euphausia superba*) around the Northern Antarctic Peninsula. *Front Mar Sci* 8:604043. <https://doi.org/10.3389/fmars.2021.604043>
- Ricketts C, Watkins JL, Priddle J, Morris DJ, Buchholz F (1992) An assessment of the biological and acoustic characteristics of swarms of Antarctic krill. *Deep Sea Res* 39:359–371
- Rösch A, Schmidbauer H (2018) WaveletComp: computational wavelet analysis. R package version 1.1. <https://CRAN.R-project.org/package=WaveletComp>
- Ross RM, Quetin LB, Lascara CM (1996) Distribution of Antarctic krill and dominant zooplankton west of the Antarctic Peninsula. In: Hofmann EE, Ross RM, Quetin LB (eds) Antarctic research series. American Geophysical Union, Washington, DC, pp 199–217. <https://doi.org/10.1029/AR070p0199>
- Sakamoto KQ, Takahashi A, Iwata T, Trathan PN (2009) From the eye of the albatrosses: a bird-borne camera shows an association between albatrosses and a killer whale in the Southern Ocean.

- PLoS ONE 4:e7322. <https://doi.org/10.1371/journal.pone.0007322>
- Santa Cruz F, Ernst B, Arata JA, Parada C (2018) Spatial and temporal dynamics of the Antarctic krill fishery in fishing hotspots in the Bransfield Strait and South Shetland Islands. *Fish Res* 208:157–166. <https://doi.org/10.1016/j.fishres.2018.07.020>
- Santora J, Veit R (2013) Spatio-temporal persistence of top predator hotspots near the Antarctic Peninsula. *Mar Ecol Prog Ser* 487:287–304. <https://doi.org/10.3354/meps10350>
- Santora JA, Reiss CS, Cossio AM, Veit RR (2009) Interannual spatial variability of krill (*Euphausia superba*) influences seabird foraging behavior near Elephant Island, Antarctica. *Fish Oceanogr* 18:20–35
- Santora JA, Reiss CS, Loeb VJ, Veit RR (2010) Spatial association between hotspots of baleen whales and demographic patterns of Antarctic krill *Euphausia superba* suggests size-dependent predation. *Mar Ecol Prog Ser* 405:255–269. <https://doi.org/10.3354/meps08513>
- Schlitzer R (2020) Ocean data view. <http://odv.awi.de>
- Schloerke B, Cook D, Larmarange J, Briatte F, Marbach M, Thoen E, Elberg A, Crowley J (2021) GGally: extension to 'ggplot2'. R package version 2.1.2 <https://CRAN.R-project.org/package=GGally>
- Schmidt K, Atkinson A, Petzke K-J, Voss M, Pond DW (2006) Protozoans as a food source for Antarctic krill, *Euphausia superba*: complementary insights from stomach content, fatty acids, and stable isotopes. *Limnol Oceanogr* 51:2409–2427. <https://doi.org/10.4319/lo.2006.51.5.2409>
- Schreer JF, Kovacs KM, O'Hara Hines RJ (2001) Comparative diving patterns of pinnipeds and seabirds. *Ecol Monogr* 71:137–162. [https://doi.org/10.1890/0012-9615\(2001\)071\[0137:CDPOPA\]2.0.CO;2](https://doi.org/10.1890/0012-9615(2001)071[0137:CDPOPA]2.0.CO;2)
- SG-ASAM (2005) Report of the first meeting of the subgroup on acoustic survey and analysis methods, La Jolla, 31 May to 2 June 2005
- SG-ASAM (2017) Report of the meeting of the subgroup on acoustic survey and analysis methods, Qingdao, 15 to 19 May 2017
- Shapiro SS, Wilk MB (1965) An analysis of variance test for normality (complete samples). *Biometrika* 52:591–611. <https://doi.org/10.2307/2333709>
- Siegel V (2005) Distribution and population dynamics of *Euphausia superba*: summary of recent findings. *Polar Biol* 29:1–22. <https://doi.org/10.1007/s00300-005-0058-5>
- Siegel V, Loeb V (1995) Recruitment of Antarctic krill *Euphausia superba* and possible causes for its variability. *Mar Ecol Prog Ser* 123:45–56
- Strycker N, Wethington M, Borowicz A, Forrest S, Witharana C, Hart T, Lynch HJ (2020) A global population assessment of the Chinstrap penguin (*Pygoscelis antarctica*). *Sci Rep* 10:19474. <https://doi.org/10.1038/s41598-020-76479-3>
- Tarling GA, Klevjer T, Fielding S, Watkins J, Atkinson A, Murphy E, Korb R, Whitehouse M, Leaper R (2009) Variability and predictability of Antarctic krill swarm structure. *Deep Sea Res Part Oceanogr Res Pap* 56:1994–2012. <https://doi.org/10.1016/j.dsr.2009.07.004>
- Tien JH, Levin SA, Rubenstein DI (2004) Dynamics of fish shoals: identifying key decision rules. *Evol Ecol Res* 6:555–565
- Torrence C, Compo GP (1998) A practical guide to wavelet analysis. *Bull Am Meteorol Soc* 79:61–78
- Tovar-Sanchez A, Duarte CM, Hernández-León S, Sañudo-Wilhelmy SA (2007) Krill as a central node for iron cycling in the Southern Ocean. *Geophys Res Lett* 34:L11601. <https://doi.org/10.1029/2006GL029096>
- Tovar-Sanchez A, Duarte CM, Hernández-León S, Sañudo-Wilhelmy SA (2009) Impact of submarine hydrothermal vents on the metal composition of krill and its excretion products. *Mar Chem* 113:129–136. <https://doi.org/10.1016/j.marchem.2009.01.010>
- Trathan PN, Brierley AS, Brandon MA, Bone DG, Goss C, Grant SA, Murphy EJ, Watkins JL (2003) Oceanographic variability and changes in Antarctic krill (*Euphausia superba*) abundance at South Georgia. *Fish Oceanogr* 12:569–583
- Trivelpiece WZ, Trivelpiece SG, Volkman NJ (1987) Ecological segregation of Adelie, Gentoo, and Chinstrap penguins at King George Island, Antarctica. *ESA* 68:351–361
- Urmey SS, Horne JK, Barbee DH (2012) Measuring the vertical distributional variability of pelagic fauna in Monterey Bay. *ICES J Mar Sci* 69:184–196. <https://doi.org/10.1093/icesjms/ifsr205>
- Viviant M, Monestiez P, Guinet C (2014) Can we predict foraging success in a marine predator from dive patterns only? Validation with prey capture attempt data. *PLoS ONE* 9:e88503
- Ward JH (1963) Hierarchical grouping to optimize an objective function. *J Am Stat Assoc* 58:236–244
- Watkins J, Brierley AS (2002) Verification of the acoustic techniques used to identify Antarctic krill. *ICES J Mar Sci* 59:1326–1336. <https://doi.org/10.1006/jmsc.2002.1309>
- Watters GM, Hill SL, Hinke JT, Matthews J, Reid K (2013) Decision-making for ecosystem-based management: evaluating options for a krill fishery with an ecosystem dynamics model. *Ecol Appl* 23:710–725. <https://doi.org/10.1890/12-1371.1>
- Weinstein BG, Double M, Gales N, Johnston DW, Friedlaender AS (2017) Identifying overlap between humpback whale foraging grounds and the Antarctic krill fishery. *Biol Conserv* 210:184–191. <https://doi.org/10.1016/j.biocon.2017.04.014>
- Wilson RP (2010) Resource partitioning and niche hyper-volume overlap in free-living Pygoscelid penguins. *Funct Ecol* 24:64–657. <https://doi.org/10.1111/j.1365-2435.2009.01654.x>
- Wood SN (2011) Fast stable restricted maximum likelihood and marginal likelihood estimation of semiparametric generalized linear models. *J R Stat Soc* 73:3–36
- Zhou M, Niiler PP, Hu JH (2002) Surface currents in the Bransfield and Gerlache straits, Antarctica. *Deep Sea Res Part I* 49:267–280
- Zhou M, Niiler PP, Zhu Y, Dorland RD (2006) The western boundary current in the Bransfield Strait, Antarctica. *Deep Sea Res Part I* 53:1244–1252

Publisher's Note Springer Nature remains neutral with regard to jurisdictional claims in published maps and institutional affiliations.

Springer Nature or its licensor (e.g. a society or other partner) holds exclusive rights to this article under a publishing agreement with the author(s) or other rightsholder(s); author self-archiving of the accepted manuscript version of this article is solely governed by the terms of such publishing agreement and applicable law.